

Supporting Information

A non-fullerene acceptor based on alkylphenyl substituted benzodithiophene for high efficiency polymer solar cells with a small voltage loss and excellent stability

Qing Guo,^a Xiaoqian Zhu,^a Xingliang Dong,^a Qinglian Zhu,^b Jin Fang,^a Xia Guo,^a Wei Ma^b, Maojie Zhang*^a and Yongfang Li^{a,c}

^a Laboratory of Advanced Optoelectronic Materials, College of Chemistry, Chemical Engineering and Materials Science, Soochow University, Suzhou 215123, China

^b State Key Laboratory for Mechanical Behavior of Materials, Xi'an Jiaotong University, Xi'an 710049, China

^c Beijing National Laboratory for Molecular Sciences, CAS Key Laboratory of Organic Solids, Institute of Chemistry, Chinese Academy of Sciences, Beijing 100190, China

Experimental Section

Instruments and Measurements

¹H NMR and ¹³C NMR spectra were measured in CDCl₃ on Bruker AV 400 MHz FT-NMR spectrometer. Elemental analysis was carried out on a flash EA1112 analyzer. Thermogravimetric analysis (TGA) was performed on a Perkin-Elmer TGA-7. UV-vis absorption spectra were taken on an Agilent Technologies Cary Series UV-Vis-NIR Spectrophotometer. The electrochemical cyclic voltammetry (CV) was performed on a Zahner Ennium IM6 Electrochemical Workstation with glassy carbon disk, Pt wire, and Ag/Ag⁺ electrode as working electrode, counter electrode, and reference electrode respectively, in a 0.1 M tetrabutylammonium hexafluorophosphate (Bu₄NPF₆) acetonitrile solution. Photoluminescence (PL) spectra was performed on an Edinburgh Instrument FLS 980. The GIWAXS measurements were performed at beamline 7.3.3 at the Advanced Light Source (ALS). Samples were prepared on a Si substrate under the same conditions as those used for device fabrication. The 10 KeV X-ray beam was incident at a grazing angle of 0.11°-0.15°, which maximized the scattering intensity from the samples. The scattered x-rays were detected using a Dectris Pilatus 2M photon counting detector. RSoXS transmission measurements were performed at beamline 11.0.1.2 at the Advanced Light Source (ALS). Samples for R-SoXS measurements were prepared on a PSS modified Si substrate under the same conditions as those used for device fabrication, and then transferred by floating in water to a 1.5 mm × 1.5 mm, 100 nm thick Si₃N₄ membrane supported by a 5 mm × 5 mm, 200 μm thick Si frame (Norcada Inc.). 2-D scattering patterns were collected on an in-vacuum CCD camera (Princeton Instrument PI-MTE). The sample detector distance was calibrated from diffraction peaks of a triblock copolymer poly(isoprene-bstyrene-b-2-vinyl pyridine), which has a known spacing of 391 Å. The beam size at the sample is approximately 100 μm by 200 μm. The FTIR

measurements were performed using a VERTEX-70V spectrometer (Bruker Optik GmbH). Films of PM6 or BP-4F were coated on Si substrates and kept under nitrogen atmosphere and degraded under the same conditions with the full devices.

The current density-voltage (J - V) characteristics of the PSCs were recorded with a Keithley 2450. The power conversion efficiencies of the PSCs were measured under 1 sun, AM 1.5G (air mass 1.5 global) (100 mW cm⁻²) using a SS-F5-3A (Enli Technology CO., Ltd.) solar simulator (AAA grade, 50 mm x 50 mm photo-beam size). 2×2 cm² Monocrystalline silicon reference cell (SRC-00019) was purchased from Enli Technology CO., Ltd. The photo-stability was measured by glove-box integrated photovoltaic performance decay testing system PVL-T-G8001M-16A (Suzhou D&R Instruments Co., Ltd.). The EQE was measured by Solar Cell Spectral Response Measurement System QE-R3011 (Enli Technology CO., Ltd.). The light intensity at each wavelength was calibrated with a standard single-crystal Si photovoltaic cell. Atomic force microscopy (AFM) measurements were performed on a Dimension 3100 (Veeco) Atomic Force Microscope in the tapping mode. Transmission electron microscopy (TEM) was performed using a TePNaï G2 F20 S-TWIN instrument at 200 kV accelerating voltage, in which the blend films were prepared using a processing technique, as following: first, the blend films were spin-cast on the PFN/ZnO/ITO substrates; second, the resulting blend film/PFN/ZnO/ITO substrates were submerged in deionized water to make these blend films float onto the air-water interface; finally, the floated blend films were taken up on unsupported 200 mesh copper grids for a TEM measurement.

Device fabrication and characterization

The PSCs devices were fabricated with an inverted device structure of ITO/ZnO/PFN-Br/PM6:BP-4F/MoO₃/Ag, which were fabricated and characterized in a N₂-filled glovebox. The ITO-coated glass substrate was cleaned with deionized water, acetone, and isopropanol, respectively. Subsequently, the pre-cleaned ITO-coated glass substrate was treated by UV-ozone for 20 min. Then, the ZnO precursor was spin-coated onto the pre-cleaned ITO glass at 2000 rpm for 60 s. For the modified ZnO layer, we spin coated PFN-Br with a speed of 2500 rpm for 30 s. The active layer was deposited by spin-coating a hot chlorobenzene solution (dissolved 12 h under 60 °C) of PM6:BP-4F with a blend concentration of 22 mg/mL inside a nitrogen box containing less than 5 ppm oxygen and moisture. Finally, 10 nm MoO₃ and 100 nm Al were sequentially evaporated on the active layer in the vacuum chamber under a pressure of *ca.* 1 × 10⁻⁴ Pa. Unless stated, the effective area of one cell is 0.04 cm². The solar cells were encapsulated with pre-cleaned glass slides using a UV-curable epoxy (DELO, LP4224) in N₂-filled glovebox. The study of stability in air is performed under a temperature of *ca.* 27 °C and a relative humidity of *ca.* 30%.

Mobility measurement

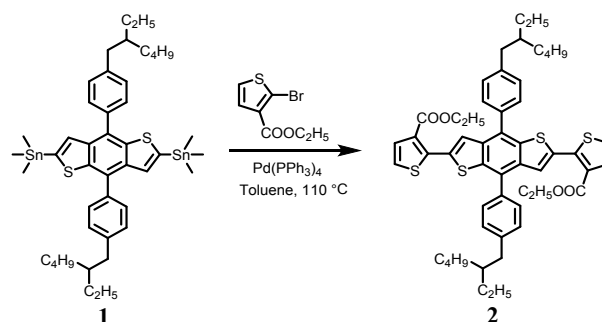
The hole and electron mobilities were calculated by using the space-charge-limited current (SCLC) method.

$$J = 9\epsilon_0\epsilon_r\mu(V_{\text{appl}} - V_{\text{bi}} - V_s)^2/8L^3$$

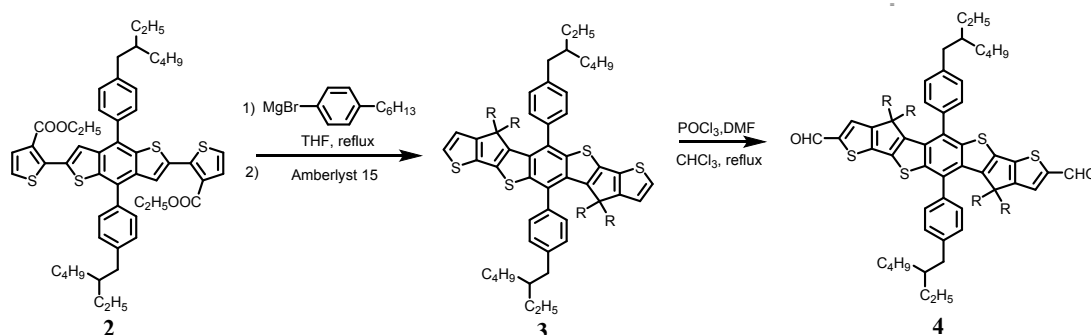
Where J is the current density, ϵ_0 is the permittivity of free space (8.85×10⁻¹² F m⁻¹), ϵ_r is the relative permittivity of the material (assumed to be 3), μ is the mobility of hole or electron, V_{appl} is the applied voltage, V_{bi} is the built-in voltage (0V), V_s is the voltage drop from the substrate's series resistance ($V_s = IR$) and L is the thickness of the active layer.

Materials and synthesis

Materials: Commercially available reagents were used without further purification. Solvents were dried and distilled from appropriate drying agents prior to use. Compound 1 were synthesized according to reported method.^[1] compound 2 (diethyl 2,2'-(4,8-bis(4-(2-ethylhexyl)phenyl)benzo[1,2-b:4,5-b']dithiophene-2,6-diyl)bis(thiophene-3-carboxylate)), compound 3, compound 4 and **BP-4F** were synthesized as follows:



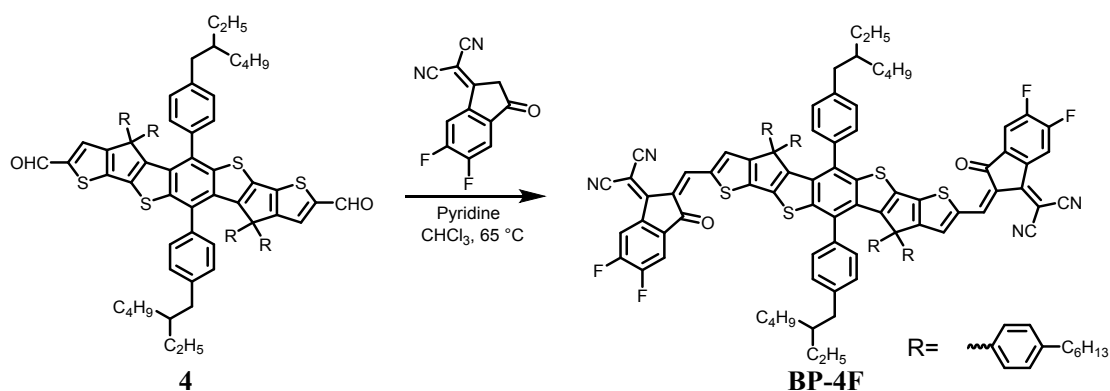
Compound 2. To a two-necked round bottom flask were added compound 1 (2.24 g, 2.5 mmol), ethyl 2-bromothiophene-3-carboxylate (1.81 g, 7.5 mmol), and toluene (100 mL). The mixture was deoxygenated with argon for 30 min. Pd(PPh₃)₄ (289 mg, 0.25 mmol) was added under argon. The mixture was refluxed at 110 °C for 24 h and then cooled down to room temperature. Water (100 mL) was added and the mixture was extracted with dichloromethane (2×100 mL). The organic phase was dried over anhydrous MgSO₄ and filtered. After removing the solvent from filtrate, the residue was purified by column chromatography on silica gel using dichloromethane/petroleum ether (1:1) as eluent yielding an orange sticky solid (1.86 g, 85%). ¹H NMR (400 MHz, CDCl₃), δ (ppm): 7.63 (dd, 6H), 7.49 (d, 2H), 7.35 (t, 4H), 7.24 (d, 2H), 4.22 (q, 4H), 1.58 (s, 4H), 1.45-1.22 (m, 18H), 1.15 (t, 6H), 1.01-0.80 (m, 12H). ¹³C NMR (100 MHz, CDCl₃), δ 163.04, 142.19, 139.07, 136.58, 135.95, 134.86, 130.68, 130.31, 129.63, 129.34, 129.00, 125.01, 60.81, 41.05, 40.04, 32.41, 28.88, 25.51, 23.02, 14.14, 13.95, 10.82; MALDI-TOF-MS m/z: [M⁺] calcd. for C₅₂H₅₈O₄S₄, 874.32; found, 874.21.



Compound 3. To a two-necked round bottom flask were added compound 2 (1.05 g, 0.12 mmol) and THF (20 mL). The mixture was deoxygenated with argon for 30 min. A THF solution (15 mL) of fresh 4-hexylphenyl-1-magnesium bromide which prepared from magnesium turnings (356mg, 1.44mmol) and 1-bromo-4-hexylbenzene (2.89 g, 1.2 mmol) was added dropwise to the mixture. The mixture was refluxed for 12 h and then cooled down to room temperature. A saturated NH₄Cl aqueous solution was added and the mixture was extracted with dichloromethane (2 × 50 mL). After removing the solvent, the yellow residue was added into a two-necked round

bottom flask. Toluene (80 mL) and Amberlyst 15 (1.2 g) were added and the mixture was deoxygenated with argon for 30 min. The mixture was refluxed at 110 °C for 12 h, then cooled down to room temperature and filtered. After removing the solvent from filtrate, the residue was purified by column chromatography on silica gel using petroleum ether as eluent yielding a light yellow crude product, which was used directly for the next step.

Compound 4. DMF (5 mL) was slowly injected into phosphorus oxychloride (4 mL) at 0 °C. After stirring for 1 hour, crude product of compound 3 (250 mg) in chloroform (25 mL) was added. The mixture was refluxed at 75 °C for 12 h, then the reaction was quenched with aqueous sodium succinate, and extracted with dichloromethane. After removing the solvent from filtrate, the residue was purified by column chromatography on silica gel using petroleum ether/dichloromethane (1:1) as eluent yielding a yellow solid (339 mg, 34%). ¹H NMR (400 MHz, CDCl₃), δ (ppm): 9.53 (s, 2H), 6.82 (s, 8H), 6.67 (d, 16H), 2.49 (s, 12H), 1.51 (d, 12H), 1.49 (s, 20H), 1.27 (s, 24H), 0.92 (s, 12H), 0.83 (s, 14H). ¹³C NMR (100 MHz, CDCl₃), δ 182.47, 164.60, 155.06, 145.82, 145.55, 144.15, 141.58, 141.48, 141.44, 135.13, 132.20, 130.94, 129.69, 128.41, 128.15, 127.84, 127.64, 41.39, 40.12, 35.47, 32.50, 31.78, 31.55, 29.68, 29.48, 29.10, 28.96, 27.19, 25.51, 23.18, 22.62, 14.30, 14.12, 10.91; MALDI-TOF-MS m/z: [M⁺] calcd. for C₉₈H₁₁₄O₂S₄, 1451.77; found, 1451.84.



BP-4F. To a two-necked round bottom flask were added compound 4 (130 mg, 0.09 mmol), 2-(5,6-difluoro-3-oxo-2,3-dihydro-1H-inden-1-ylidene)malononitrile (87 mg, 0.45 mmol), chloroform (30 mL), and 1.0 mL pyridine. The mixture was deoxygenated with argon for 30 min and then refluxed for 12 h. After cooling down to room temperature, the mixture was poured into methanol (200 mL) and filtered. The residue was purified by column chromatography on silica gel using dichloromethane/ petroleum ether (1:2) as eluent yield a blue solid (143 mg, 89%). ¹H NMR (400 MHz, CDCl₃), δ (ppm): 8.56 (s, 2H), 8.48 -8.32 (m, 2H), 7.52 (dd, 2H), 6.85 (s, 8H), 6.78-6.55 (m, 16H), 2.51 (d, 12H), 1.55 (s, 12H), 1.29 (dd, 38H), 0.94 (d, 12H), 0.84 (s, 12H). ¹³C NMR (100 MHz, CDCl₃), δ 185.82, 165.75, 158.09, 154.50, 153.43, 150.31, 141.84, 140.81, 138.19, 134.49, 134.31, 133.79, 133.21, 130.69, 130.16, 128.54, 128.23, 120.38, 114.85, 114.28, 112.50, 77.19, 76.98, 76.77, 68.69, 41.34, 40.10, 35.48, 32.52, 31.78, 31.54, 29.91, 28.92, 25.43, 23.22, 22.66, 14.34, 14.13, 10.91; MALDI-TOF-MS m/z: [M⁺] calcd. for C₁₂₂H₁₁₈F₄O₂S₄, 1875.81; found, 1875.53.

Supplementary figures and tables

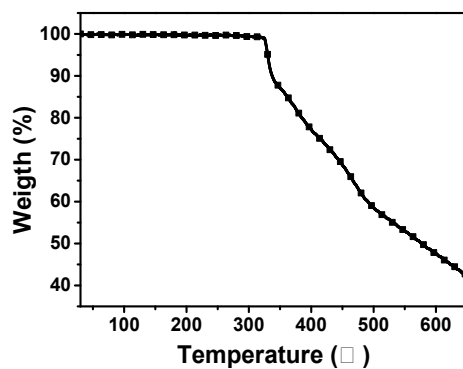


Fig. S1 TGA plot of BP-F with a heating rate of $10\text{ }^{\circ}\text{C min}^{-1}$ under nitrogen atmosphere.

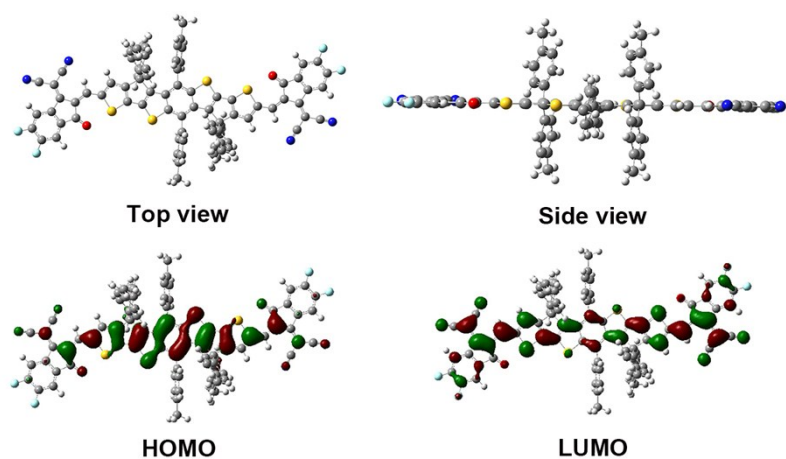


Fig. S2 The optimal geometries and LUMO, HOMO, and distribution of BP-4F (alkyl chains are simplified to methyl) calculated at B3LYP/6-31G** level

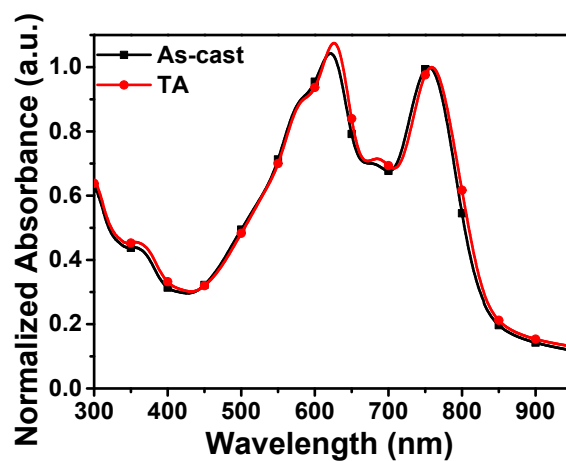


Fig. S3 The absorption spectra of PM6:BP-4F-based blend film

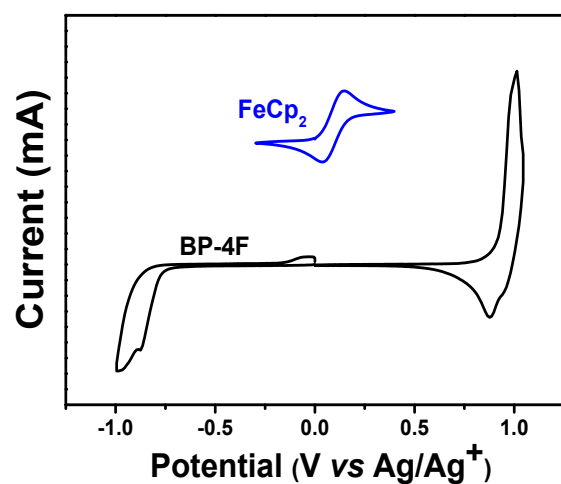


Fig. S4 Cyclic voltammetry for BP-4F.

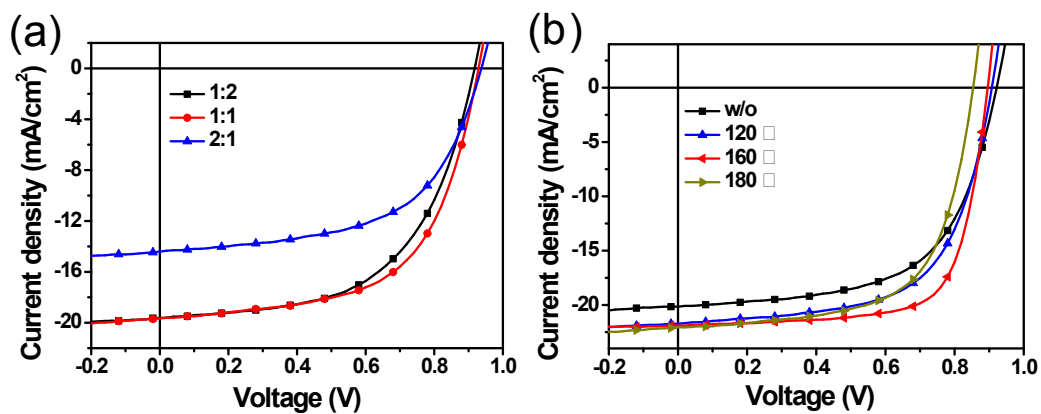


Fig. S5 J-V curves curves of solar cells (a) with different PM6:BP-4F blend ratios and (b) based on PM6:BP-4F (1:1, w/w) blend with different thermal annealing treatment for 10 min.

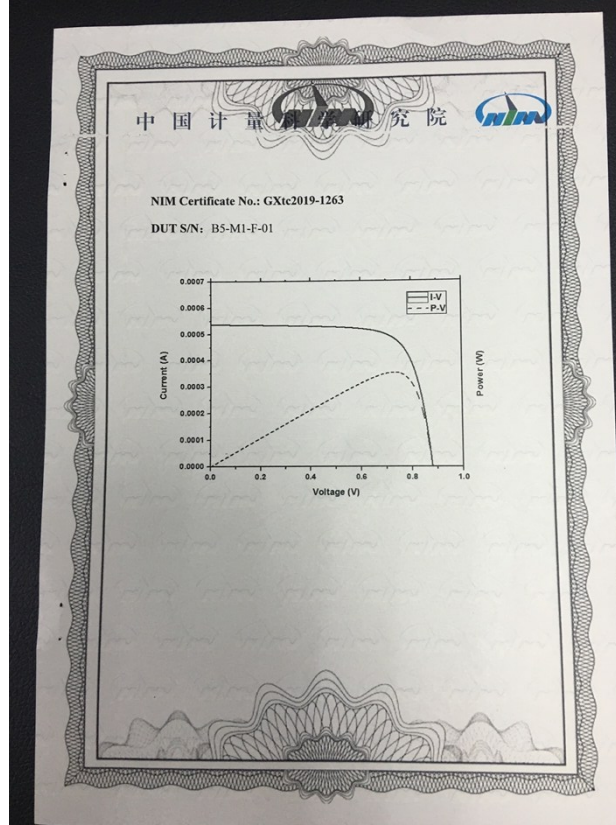
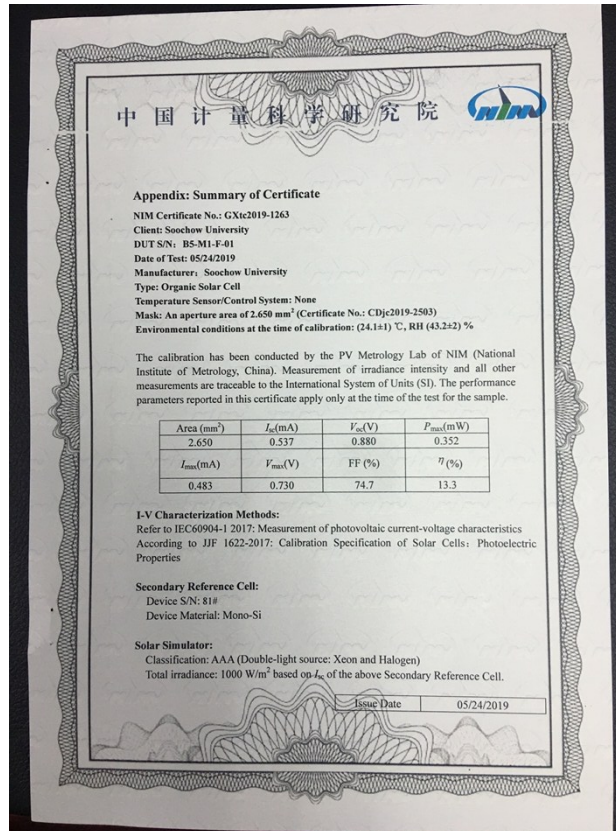


Fig. S6 Test report of the PM6:BP-4F-based PSCs from National Institute of Metrology, China (NIM).

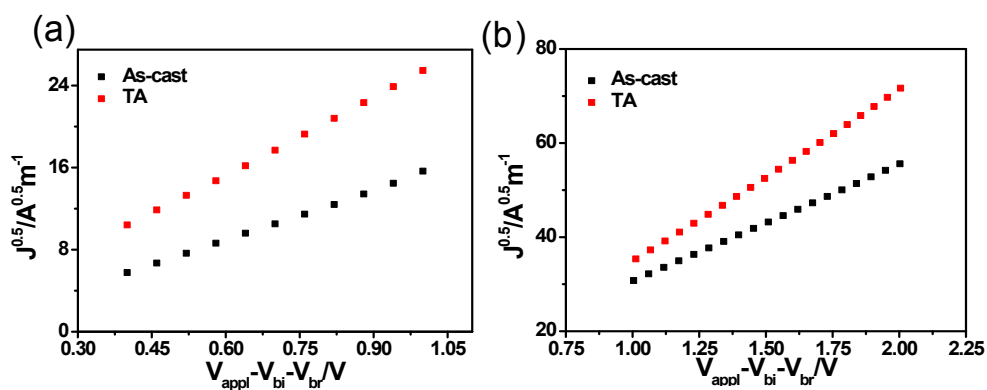


Fig. S7 (a) Electron mobilities of corresponding devices, (b) Hole mobilities of corresponding devices.

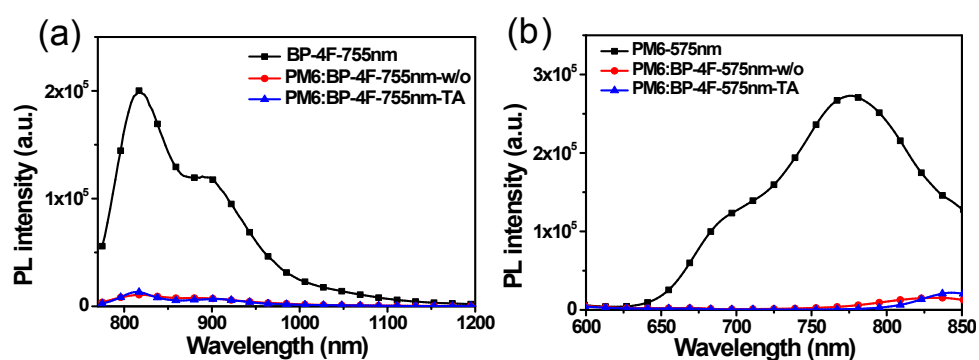


Fig. S8 PL spectra of the (a) BP-4F and (b) PM6 pure films and their blends.

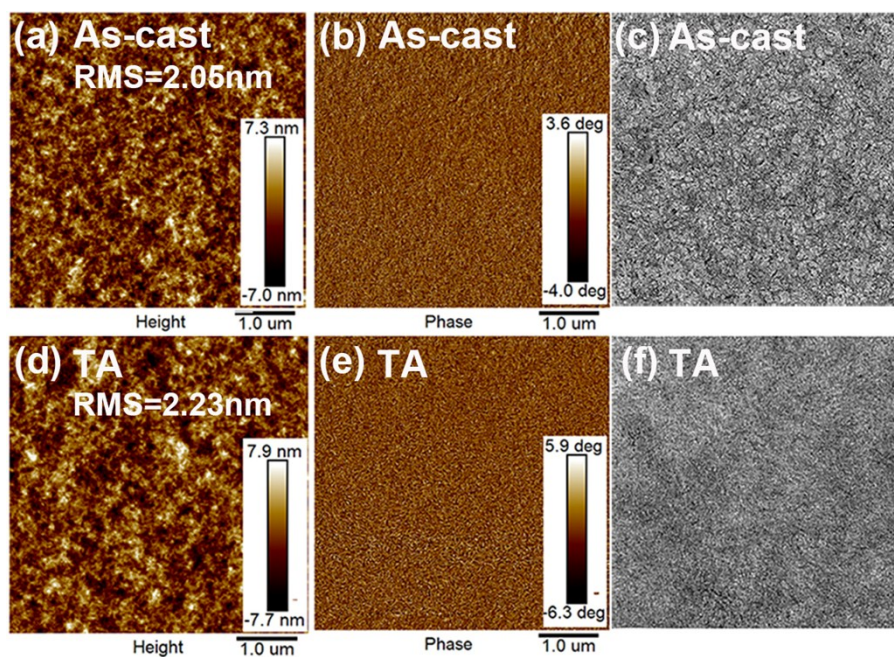


Fig. S9 AFM images for (a), (b) the as-cast blended films and (d), (e) the TA treated blended films. TEM images for (c) the as-cast blended film and (f) the TA treated blended film.

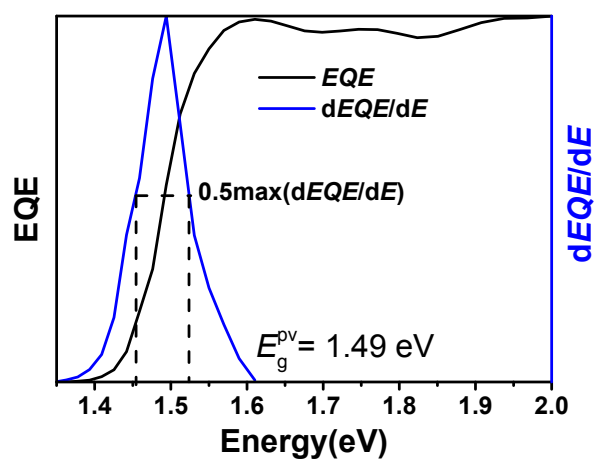


Fig. S10 Deduction of optical bandgap from the definition of E_g^{PV}

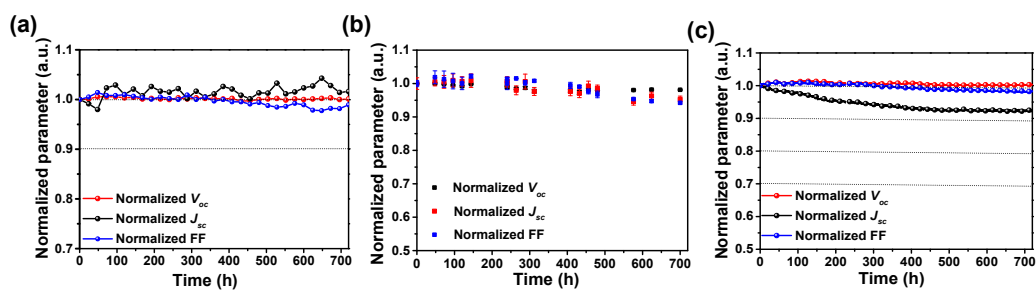


Fig. S11 Normalized parameters of devices (a) undere dark in the glove box, (b) under dark in air, and (c) under continuous illumination in glove box.

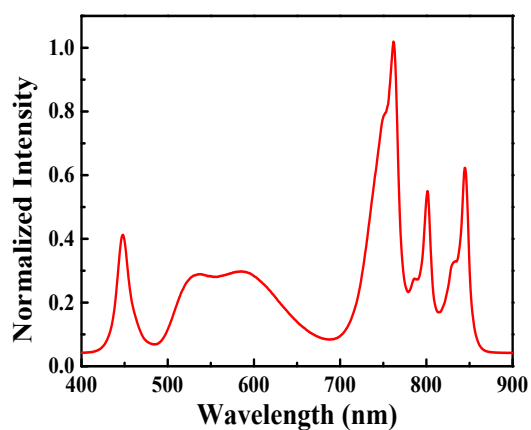


Fig. S12 Light spectrum of the LEDs used in this work.

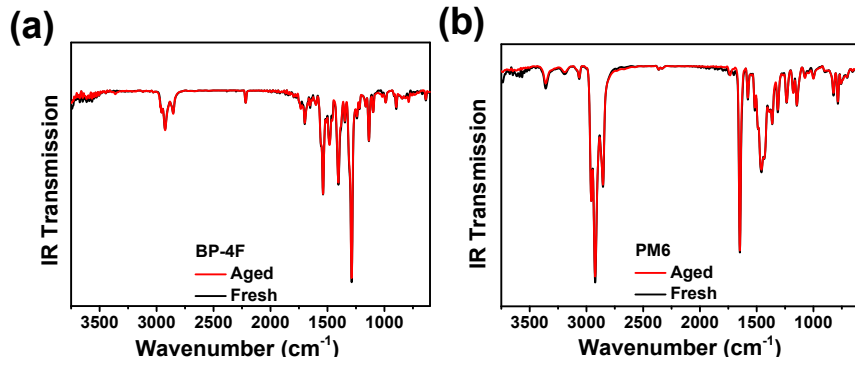


Fig. S13 The FTIR spectra of fresh and aged film based on (a) BP-4F and (b) PM6.

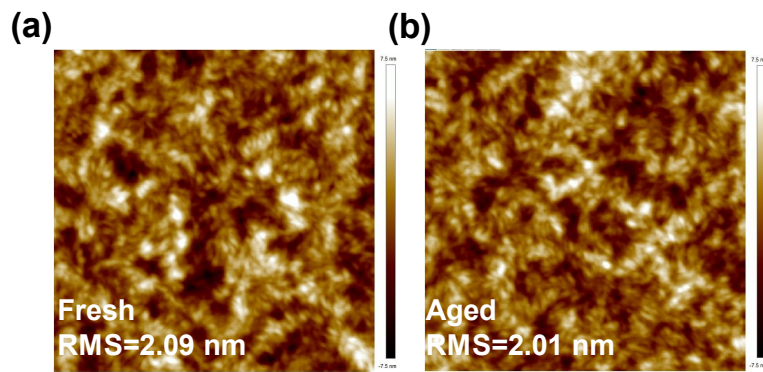


Fig. S14 AFM images for (a) Fresh blended films and (b) Aged blended films

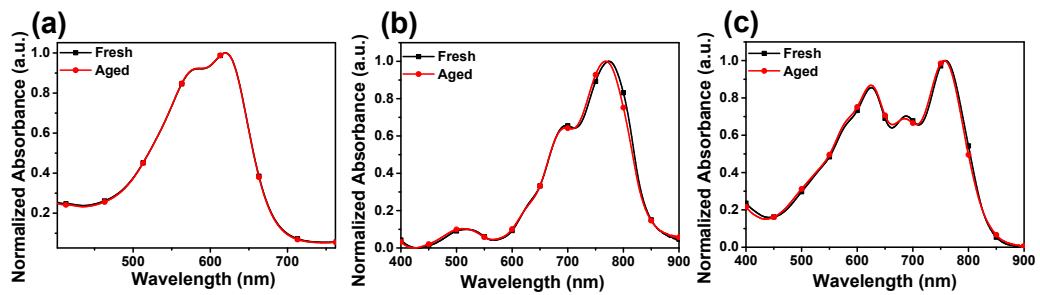


Fig. S15 Absorption spectra of fresh and aged film based on (a) PM6, (b) BP-4F, and (c) PM6:BP-4F.

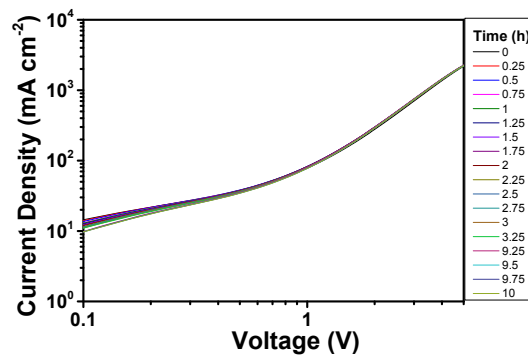


Fig. S16 Stability of electron-only devices (structure: ITO/ZnO/PM6:BP-4F/Ca/Ag) under continuous illumination under N₂ atmosphere.

Table S1. The best photovoltaic performance of solar cells with different PM6:BP-4F blend ratios under the illumination of AM 1.5 G, 100 mW cm⁻².

D:A (w/w)	V_{oc} (V)	J_{sc} (mA cm ⁻²)	FF	PCE (%)
1:2	0.92	19.6	0.57	10.2
1:1	0.92	20.2	0.60	11.2
2:1	0.94	16.8	0.59	9.1

Table S2. The best photovoltaic performance of solar cells based on PM6:BP-4F (1:1, w/w) blend with different thermal annealing treatment for 10 min.

Temperature (°C)	V_{oc} (V)	J_{sc} (mA cm ⁻²)	FF	PCE (%)
As-cast	0.92	20.2	0.60	11.2
120	0.91	21.7	0.62	12.3
160	0.90	21.9	0.72	14.2
180	0.85	22.1	0.64	12.0

Table S3. Charge mobilities of PM6:BP-4F (1:1, w/w) blend films with/without thermal annealing treatment.

	Hole mobility (cm ² V ⁻¹ s ⁻¹)	Electron mobility (cm ² V ⁻¹ s ⁻¹)
As-cast	2.72×10^{-4}	1.24×10^{-4}
TA	5.93×10^{-4}	2.81×10^{-4}

Table S4. Photovoltaic results of recent high performance PSC devices (PCE >12%) based on polymer donor and non-fullerene acceptor (NFA).

Donor	NFA	E_g^{opt} (eV)	V_{oc} (V)	E_{loss} (eV)	J_{sc} (mA cm ⁻²)	PCE _{max} (%)	Ref.
PBDTS-TDZ	ITIC	1.58	1.10	0.48	17.78	12.8	2
PM6	SeTIC4Cl	1.44	0.78	0.66	22.92	13.32	3
FTAZ	IDIC	1.62	0.84	0.78	20.8	12.5	4

PBDB-T	SN6IC-4F	1.32	0.78	0.54	23.2	13.2	5
PBDB-T	NCBDT	1.45	0.84	0.61	20.33	12.1	6
PBT1-C	TPTTT-2F	1.56	0.92	0.64	17.63	12.1	7
PBDB-T	NITI	1.49	0.86	0.63	20.67	12.7	8
FTAZ	IOIC2	1.55	0.90	0.65	19.7	12.3	9
PTB7-Th	IOIC3	1.45	0.76	0.68	22.9	13.1	10
PTB7-Th	FOIC	1.32	0.58	0.74	24.0	12.0	11
PBDB-T	ZITI	1.53	0.89	0.64	19.8	13.0	12
PM6	Y6	1.33	0.82	0.51	25.2	15.7	13
PBDB-T	INPIC-4F	1.39	0.85	0.54	21.61	13.1	14
FTAZ	IDCIC	1.45	0.87	0.58	21.98	13.6	15
PBDB-T	IT-M	1.60	0.94	0.66	17.44	12.1	16
PBDB-T-SF	IT-4F	1.54	0.88	0.66	20.50	13.1	17
PDTB-ET-T	IT-4F	1.54	0.90	0.63	20.73	14.2	18
PBDB-T-2Cl	IT-4F	1.54	0.86	0.68	21.80	14.4	19
J71	ITCF	1.57	0.91	0.666	18.48	13.3	20
PBDB-T-2F	IT-4Cl	1.48	0.79	0.69	22.67	13.5	21
PBT1-C	ITCPTC	1.58	0.94	0.64	17.0	12.7	22
J71	MeIC	1.65	0.92	0.73	18.41	12.5	23
PBDB-T	ITOIC-2F	1.45	0.90	0.55	21.04	12.2	24
PBDB-T	IDTOT2F	1.44	0.85	0.59	20.87	12.8	25
PPBDB-TF	IDIC-C4Ph	1.62	0.94	0.68	19.06	14.0	26
PFBDB-T	C8-ITIC	1.55	0.94	0.61	19.6	13.2	27
PTB7-Th	IOTIC-2F	1.31	0.82	0.49	21.9	12.1	28
PDTB-ET-T(P ₂)	IT-4F	1.54	0.90	0.64	20.7	14.2	29
PBDB-TF	IT-4F	1.54	0.87	0.67	20.7	14.6	30
PBDB-T-SF	NCBDT-4Cl	1.40	0.85	0.55	22.3	14.1	31

T1	IT-4F	1.54	0.9	0.64	21.5	15.1	32
PBDB-TF	AT-4Cl	1.60	0.90	0.70	19.52	13.3	33
PM6	BP-4F	1.49	0.90	0.59	21.9	14.2	This work

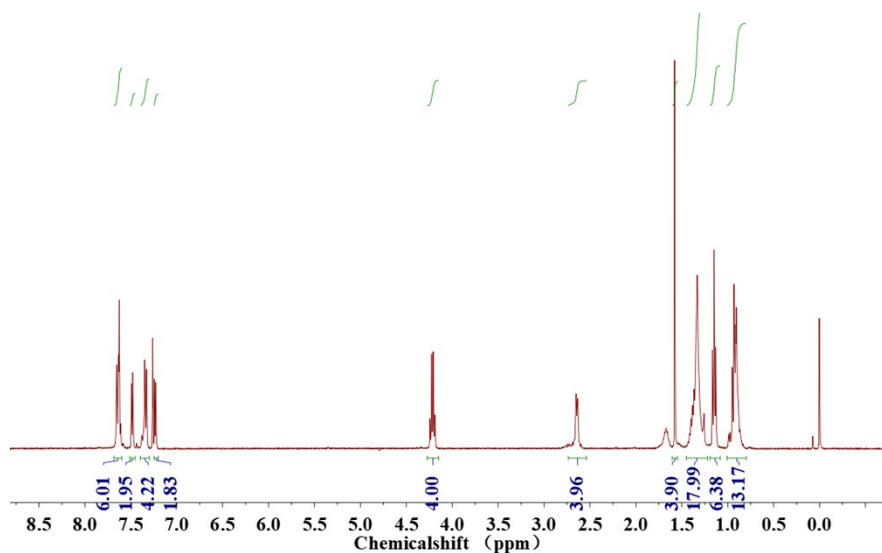


Fig. S17 ¹H NMR spectra of compound 2 in CDCl₃.

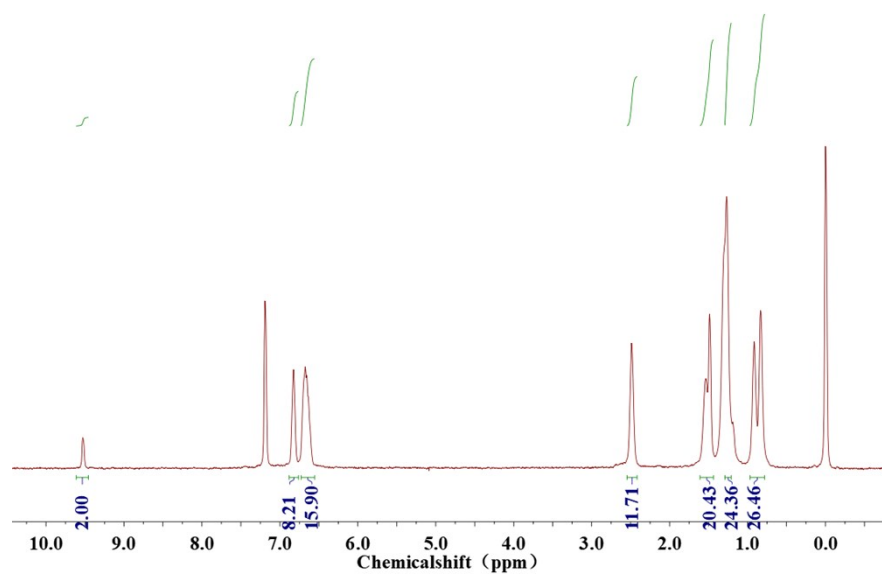


Fig. S18 ¹H NMR spectra of compound 4 in CDCl₃.

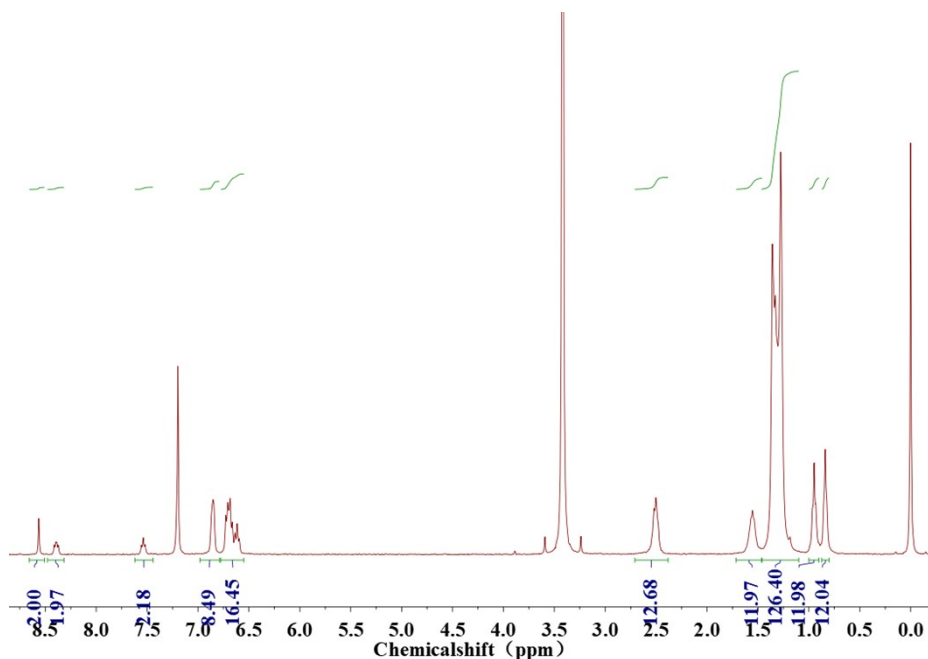


Fig. S19 ^1H NMR spectra of BP-4F in CDCl_3

References

1. M. Zhang, Y. Gu, X. Guo, F. Liu, S. Zhang, L. Huo, T. P. Russell and J. Hou, *Adv. Mater.* 2013, **25**, 4944.
2. X. Xu, T. Yu, Z. Bi, W. Ma, Y. Li and Q. Peng, *Adv. Mater.*, 2018, **30**, 1703973.
3. J. Wang, K. Liu, L. Hong, G. Ge, C. Zhang and J. Hou, *ACS Energy Lett.*, 2018, **3**, 2967.
4. Y. Lin, F. Zhao, S. K. Prasad, J. Chen, W. Cai, Q. Zhang, K. Chen, Y. Wu, W. Ma, F. Gao, J. Tang, C. Wang, W. You, J. M. Hodgkiss and X. Zhan, *Adv. Mater.*, 2018, **30**, 1706363.
5. C. Huang, X. Liao, K. Gao, L. Zuo, F. Lin, X. Shi, C. Li, H. Liu, X. Li, F. Liu, Y. Chen, H. Chen and A. K.-Y. Jen, *Chem. Mater.*, 2018, **30**, 5429.
6. B. Kan, J. Zhang, F. Liu, X. Wan, C. Li, X. Ke, Y. Wang, H. Feng, Y. Zhang, G. Long, R. H. Friend, A. A. Bakulin, Y. Chen, *Adv. Mater.* 2018, **30**, 1704904.
7. J. Song, C. Li, L. Ye, C. Koh, Y. Cai, D. Wei, H. Y. Woo and Y. Sun, *J. Mater. Chem. A*, 2018, **6**, 18847.
8. S. j. Xu, Z. Zhou, W. Liu, Z. Zhang, F. Liu, H. Yan, X. Zhu, *Adv. Mater.* 2017, **29**, 1704510.
9. J. Zhu, Z. Ke, Q. Zhang, J. Wang, S. Dai, Y. Wu, Y. Xu, Y. Lin, W. Ma, W. You and X. Zhan, *Adv. Mater.* 2018, **30**, 1704713.
10. J. Zhu, Y. Xiao, J. Wang, K. Liu, H. Jiang, Y. Lin, X. Lu and X. Zhan, *Chem. Mater.*, 2018, **30**, 4150.
11. T. Li, S. Dai, Z. Ke, L. Yang, J. Wang, C. Yan, W. Ma and X. Zhan, *Adv. Mater.*, 2018, **30**, 1705969.
12. W. Liu, J. Zhang, Z. Zhou, D. Zhang, Y. Zhang, S. Xu and X. Zhu, *Adv. Mater.*, 2018, **30**, 1800403.
13. J. Yuan, Y. Zhang, L. Zhou, G. Zhang, H.-L. Yip, T.-K. Lau, X. Lu, C. Zhu, H. Peng, P. A. Johnson, M. Leclerc, Y. Cao, J. Ulanski, Y. Li and Y. Zou, *Joule*, 2019, DOI: 10.1016/j.joule.2019.01.004.
14. J. Sun, X. Ma, Z. Zhang, J. Yu, J. Zhou, X. Yin, L. Yang, R. Geng, R. Zhu and F. Zhang, *Adv. Mater.*, 2018, **30**, 1707150.
15. D. He, F. Zhao, J. Xin, J. J. Rech, Z. Wei, W. Ma, W. You, B. Li, L. Jiang, Y. Li and C. Wang, *Adv. Energy Mater.*, 2018, **8**, 1802050.
16. S. Li, L. Ye, W. Zhao, S. Zhang, S. Mukherjee, H. Ade and J. Hou, *Adv. Mater.*, 2016, **28**, 9423.
17. W. Zhao, S. Li, H. Yao, S. Zhang, Y. Zhang, B. Yang and J. Hou, *J. Am. Chem. Soc.*, 2017, **139**, 7148.

18. S. Li, L. Ye, W. Zhao, H. Yan, B. Yang, D. Liu, W. Li, H. Ade and J. Hou, *J. Am. Chem. Soc.*, 2018, **140**, 7159.
19. S. Zhang, Y. Qin, J. Zhu and J. Hou, *Adv. Mater.*, 2018, **30**, 1800868.
20. M. Hao, T. Liu, Y. Xiao, L. Ma, G. Zhang, C. Zhong, Z. Chen, Z. Luo, X. Lu, H. Yan, L. Wang and C. Yang, *Chem. Mater.*, 2019, **31**, 1752.
21. H. Zhang, H. Yao, J. Hou, J. Zhu, J. Zhang, W. Li, R. Yu, B. Gao, S. Zhang and J. Hou, *Adv. Mater.*, 2018, **30**, 1800613.
22. T. Liu, L. Huo, S. Chandrabose, K. Chen, G. Han, F. Qi, X. Meng, D. Xie, W. Ma, Y. Yi, J. M. Hodgkiss, F. Liu, J. Wang, C. Yang and Y. Sun, *Adv. Mater.*, 2018, **30**, 1707353.
23. Z. Luo, H. Bin, T. Liu, Z. Zhang, Y. Yang, C. Zhong, B. Qiu, G. Li, W. Gao, D. Xie, K. Wu, Y. Sun, F. Liu, Y. Li and C. Yang, *Adv. Mater.*, 2018, **30**, 1706124.
24. Y. Liu, C. Zhang, D. Hao, Z. Zhang, L. Wu, M. Li, S. Feng, X. Xu, F. Liu, X. Chen and Z. Bo, *Chem. Mater.*, 2018, **30**, 4307.
25. Y. Liu, M. Li, X. Zhou, Q. Jia, S. Feng, P. Jiang, X. Xu, W. Ma, H. Li and Z. Bo, *ACS Energy Lett.*, 2018, **3**, 1832.
26. Y. Li, N. Zheng, L. Yu, S. Wen, C. Gao, M. Sun and R. Yang, *Adv. Mater.*, 2019, **31**, 1807832.
27. Z. Fei, F. D. Eisner, X. Jiao, M. Azzouzi, J. A. Röhr, Y. Han, M. Shahid, A. S. R. Chesman, C. D. Easton, C. R. McNeill, T. D. Anthopoulos, J. Nelson and M. Heeney, *Adv. Mater.*, 2018, **30**, 1705209.
28. J. Lee, S. J. Ko, M. Seifrid, H. Lee, C. McDowell, B. R. Luginbuhl, A. Karki, K. Cho, T. Q. Nguyen and G. C. Bazan, *Adv. Energy Mater.* 2018, **8**, 1801209.
29. S. Li, L. Ye, W. Zhao, H. Yan, B. Yang, D. Liu, W. Li, H. Ade and J. Hou, *J. Am. Chem. Soc.* 2018, **140**, 7159.
30. Z. Zheng, Q. Hu, S. Zhang, D. Zhang, J. Wang, S. Xie, R. Wang, Y. Qin, W. Li, L. Hong, N. Liang, F. Liu, Y. Zhang, Z. Wei, Z. Tang, T. P. Russell, J. Hou and H. Zhou, *Adv. Mater.* 2018, **30**, 1801801.
31. B. Kan, H. R. Feng, H. F. Yao, M. J. Chang, X. J. Wan, C. X. Li, J. H. Hou and Y. S. Chen, *Sci. China Chem.* 2018, **61**, 1307.
32. Y. Cui, H. Yao, L. Hong, T. Zhang, Y. Xu, K. Xian, B. Gao, J. Qin, J. Zhang, Z. Wei, J. Hou, *Adv Mater*, 2019, **31**, 1808356.
33. H. Feng, Y. Q. Q. Yi, X. Ke, J. Yan, Y. Zhang, X. Wan, C. Li, N. Zheng, Z. Xie and Y. Chen, *Advanced Energy Materials*, 2019, **9**, 1803541.